Subwavelength-grating contra-directional couplers for large stopband filters

Dominique Charron, Jonathan St-Yves, Omid Jafari, Sophie LaRochelle, and Wei Shi

OSA Optics Letters, (Volume 43, Issue 4) (2018)

Doi: 10.1364/OL.43.000895

https://doi.org/10.1364/OL.43.000895

Subwavelength-grating contra-directional couplers for large stopband filters

DOMINIQUE CHARRON[1], JONATHAN ST-YVES[1], OMID JAFARI[1], SOPHIE LAROCHELLE[1], AND WEI SHI[1,*]

[1] *Centre d'optique, photonique et laser (COPL) and Département de génie électrique et génie informatique, Université Laval, 2375 rue de la Terrasse, Québec G1V 0A6, Canada*
[*] *Corresponding author: wei.shi@gel.ulaval.ca*

Compiled January 12, 2018

Manipulating the coupling coefficient a t subwavelength scales provides an additional degree of freedom in designing integrated Bragg gratings. We demonstrate asymmetric contra-directional couplers (contra-DCs) using side-wall-corrugated subwavelength grating (SWG) waveguides for broadband add-drop Bragg filters. W e s how t hat S WG c an e ffectively increase the overlap of coupled modes and thus the photonic band gap. The measured spectra show good agreement with the prediction of photonic band structure simulations. A record bandwidth of 4.07 THz (33.4 nm) has been achieved experimentally. A four-port Bragg resonating filter m ade o f a p hase-shifted B ragg grating SWG contra-DC is also demonstrated for narrow-band (near 100 GHz) filtering. A ll t hese d evices are achieved on the 220-nm silicon-on-insulator platform with a compact length of less than 150 μm. These large-stopband filters m ay fi nd im portant ap plications such as band splitting, reconfigurable c hannel b and switching, bandwidth-tunable filtering a nd d ispersion engineering.

OCIS codes: (130.0130) Integrated optics; (230.5750) Resonators; (130.7408) Wavelength filtering devices; (050.6624) Subwavelength structures.

Silicon-on-insulator (SOI) is a promising platform for large-scale integration of nano-photonic devices for faster, more affordable optical communication networks. Precise and reconfigurable filtering of wavelength division multiplexed channels, either coarse or dense, allows to increase the capacity and flexibility of optical networks for broadband access. Various kinds of devices have been proposed to realize filtering on the 220-nm-thick SOI platform such as Bragg gratings [1], microring resonators [2], Mach-Zehnder interferometers [3], contra-directional couplers [4] and many others. While most of these demonstrations are narrow band, there is an interest to develop broader filter designs, from hundreds of GHz to a few THz, for applications such as bandwidth-tunable filtering [5] and dispersion engineering [6]. Few designs have been demonstrated to allow wide band filtering so far. Integrated Bragg gratings or 1D photonic crystals can be designed with very wide photonic band gap which makes them suitable for broadband filtering applications. Narrow-band filters with large stop band can also be implemented by creating phase-shifted resonators in broadband Bragg gratings, offering a more compact footprint compared to a narrow stop band design.

Grating-assisted contra-directional couplers (contra-DCs) are add-drop filters using gratings for the wavelength selectivity [7]. Similar to Bragg gratings in a single waveguide, the periodic dielectric perturbations are essential for efficient coupling between modes propagating in opposite directions. The difference is that the contra-DC drops the filtered wavelength into another waveguide. As such, no circulator is needed for the add-drop operation allowing monolithic integration with other photonic components. For optimal results, there needs to be an asymmetry in the waveguides of the coupler to suppress co-directional coupling. This ensures that the intra-waveguide Bragg reflection is far from the wavelength of operation. Typically, the asymmetry is introduced using different widths for the waveguide. As the coupling strength is dependent on the mode overlap in the coupler, it is challenging to achieve very large coupling due to the strong mode confinement in conventional SOI waveguides.

A subwavelength grating (SWG) waveguide consists of gratings with an in-line period inferior to half the operating wavelength [8]. This makes the gratings act similar to a homogeneous metamaterial waveguide with a volumetric averaged refractive index and is an effective means to engineer the mode profile and dispersion. Thanks to the smaller feature size achievable using e-beam lithography, many devices have been improved or specialized using SWG structures, such as wavelength independent coupler [9], high-efficiency edge coupler [10], and filters [11]. A SWG-analogous contra-DC have been demonstrated [12, 13], where a continuous strip waveguide is in proximity to a discontinued Bragg waveguide in which silicon and oxide alternate with a period equal to half the wavelength (Bragg condition).

In this Letter, we present a novel design of contra-DC using a SWG waveguide to generate asymmetry between two coupled waveguides, one strip waveguide and one SWG waveguide both with sidewall Bragg corrugation and having a constant waveguide width. The SWG waveguide has a period of a quarter of the wavelength, i.e., half the Bragg period. Bragg gratings are then formed by corrugating the sidewalls of both the waveguides. The use of SWG allows for an enlarged mode overlap with the

dielectric perturbation resulting in a higher coupling and thus a larger photonic band gap.

The schematic of the proposed device is shown in Fig.1. A SWG waveguide consisting of alternating subwavelength elements with lateral displacement is coupled to a strip waveguide. Corrugations are also formed on the sidewalls of the strip waveguide in phase with the SWG elements. As a result, the gap between the SWG and the strip waveguides also changes periodically for spatial coupling modulation. The pitch of the Bragg grating is chosen so that the fundamental mode of the coupler mainly confined in the strip waveguide is backward coupled to the second-order mode mainly confined in the SWG waveguide. Only quasi-TE modes are considered here. The SWG period is chosen to be half the Bragg grating period, far from the Bragg condition in the subwavelength regime.

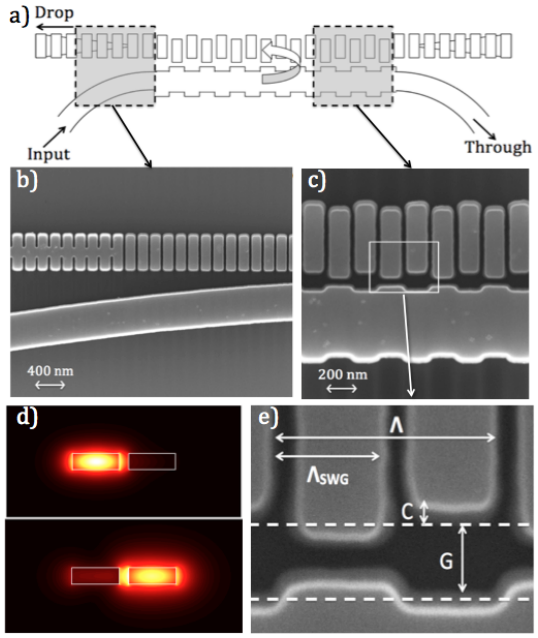

Fig. 1. (a) Schematic of the device. (b) SEM picture at the end of a triangular taper for strip to SWG regime conversion. The curved bottom waveguide gradually approaches the SWG waveguide for an adiabatic excitation of the fundamental mode. (c) The coupling region showing the sidewall corrugation in the strip waveguide and the lateral displacement in the SWG waveguide. All the SEM pictures come from the same device with a waveguide width of 500 nm, a Bragg period of 345 nm, a SWG duty cycle of 75% and a sidewall corrugation depth of 30 nm for both waveguides. (d) Simulated cross-sectional optical-field distribution of the first-order TE mode (top) mainly confined in the strip waveguide and the second-order TE mode (bottom) mainly confined in the SWG waveguide. (e) SEM picture with visual representation of the Bragg grating corrugation period Λ, of the SWG period Λ_{SWG} with duty cycle D, of the corrugation amplitude C and of the average gap between the waveguides G.

The use of SWG waveguide allows more flexibility in the design process by virtually changing the refractive index of the waveguide. However, its design and simulation are more complex. The mode propagation can be accurately described using the Bloch mode equations [14], but the easiest method, for a more efficient design process, is to approximate the grating to a strip waveguide with volumetric averaged refractive index [15]. This allows the use of the same design procedure as for a conventional contra-DC, which has been adopted in the design of our device. The method consists of extracting the modes distribution and effective index from eigenmode simulations performed with a mode solver and to extract the coupling coefficient κ through the coupled-mode overlap over the dielectric perturbation [7]. The Bragg conditions for inter-waveguide back reflection and intra-waveguide coupling can be extracted from the effective indexes. Those values are then used as inputs for the transfer matrix method (TMM) to calculate the spectral responses of the device. The TMM also allows to consider linear chirp, random phase noise, phase-shift and loss to adjust the simulation to fabrication variability [5]. However, coupling-coefficient calculation using the coupled-mode theory for gratings structure tends to overestimate the coupling coefficient due to the innate approximation of strong corrugations.

Another way to extract coupling coefficient is to perform FDTD simulation over a grating period using the Bloch boundary condition along the propagation axis to obtain the photonic band structure [16]. Such simulations are more computationally expensive, but does not require the averaged index approximation for the SWG waveguide design. From the photonic band structure, important parameters, such as effective index n_{eff}, group index n_g, photonic band gap $\Delta\lambda$ and central wavelength λ_c, can be easily extracted to calculate the coupling coefficient using $\kappa = \pi n_g \Delta\lambda / \lambda_c^2$. Fig.2 shows an example of the photonic band structure calculated for one of our designs. We can see that the spacing between the center wavelength of contra-directional coupling (λ_{CDC}) is about 100 nm away from the other Bragg wavelengths associated to intrawaveguide back reflections ($\lambda_{Bragg,SWG}$ and $\lambda_{Bragg,strip}$), ensuring single-band operation within a very wide spectral range. This method was used for the analysis of experimental results.

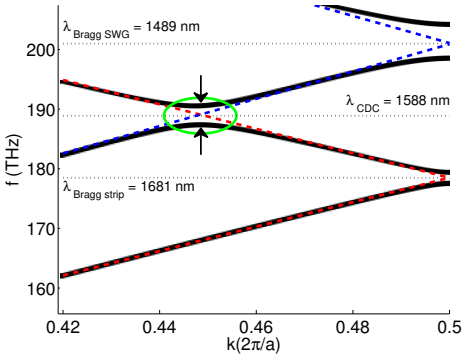

Fig. 2. Photonic band structure of a device with a period of 365 nm, a duty cycle of 75%, a gap of 100 nm, and corrugations of 30 nm. The blue line denotes the propagation along the SWG waveguide while the red line shows the propagation along the strip waveguide. The intra-waveguide Bragg reflexion occurs at the limit of first Brillouin zone of the grating, which corresponds to a wave number of 0.5 with normalization. The contra-directional coupling occurs in the green circle and corresponds to the intersection of the forward and backward propagation in each waveguide. The arrows indicate the photonic band gap $\Delta\lambda$ (27 nm) generated by the contra-directional coupling. Note that varied design parameters have been used in the experimental results shown below.

With the addition of SWG, there are more geometric parame-

ters available to optimize each design. Given that the SWG can create large asymmetry in the coupler by varying the duty cycle of the SWG, the widths of both waveguide are kept constant as 500 nm. Each design contains a coupling length of 400 periods. To generate the dielectric perturbation, the coupling region contains a uniform sidewall grating between the two waveguides, while out-of-phase gratings are formed on the external sidewalls with a mismatch of $\pi/2$ to suppress back reflection [17]. The sidewall corrugations have variations of 10, 20 and 30 nm. The variations for the average gap in between the two waveguides are 100 and 150 nm. The duty cycle of the SWG waveguide is chosen as either 60% or 75% to keep the effective index of the mode superior to 1.6 to ensure that the substrate leakage would not cause significant losses [18]. From the SEM pictures of the device shown in Fig.1, the obtained duty cycle is measured at an average of 75.4±1% for the 75% design. The SWG period Λ_{SWG} was kept at half the Bragg period Λ. For the waveguides leading in and out of the coupling region, a proximity taper and a strip to SWG taper have been used. The proximity taper consists of a bend in the strip waveguide with a radius of 42 μm. The strip to SWG taper [19] consists of 100 SWG elements overlaid with a triangular tip for a length of around 18 μm. Fiber grating coupler are used as optical inputs and outputs [20]. The devices were fabricated using e-beam lithography on the CMOS-compatible SOI platform. E-beam lithography allows for smaller feature sizes but is less suitable for mass production. A stronger smoothing effect needs to be considered in using optical lithography [21].

The measured results of a broadband filter design with a coupler gap G of 100 nm and a corrugation depth of 30 nm are plotted in Fig.3 a), showing a 3-dB bandwidth of 4.07 THz or 33.4 nm. The design also shows a good extinction ratio of over 35 dB in the through port. The through-port responses are compared for corrugations of 10 nm, 20 nm, and 30 nm and are shown in Fig.3 b). We can see that the bandwidth increases with the corrugation from 1 THz to 4.07 THz. The measurements have been normalized using the averaged response of pairs of fiber-to-waveguide grating couplers on the same chip. Since the grating is uniform without any apodization profile, the sidelobes are very strong. Future work could introduce Gaussian-profiled coupling apodization for efficient sidelobe suppression [4]. Taking into account the wafer thickness non-uniformity and etching variance, a linear chirp on the propagation constant is introduced along the longitudinal direction [22]. Another source of noise present in the simulation is the high-frequency phase noise caused by sidewall roughness [23]. It is simulated by adding a random noise on the propagation constant. For the simulation fits in this letter, the linear chirp is adjusted for each design with a maximum value used of 0.19 nm in height variation over the length of the grating structure. As for the random chirp, it is kept constant for all the devices with a maximum random amplitude corresponding to 1 nm in width variations. Both chirp values are in the same order as previous works [24, 25].

The effect of the corrugation depth is also investigated as shown in Fig.3 b). A stronger corrugation should generate a higher coupling coefficient and thus a larger bandwidth. Fig.4 a) shows the impacts of the gap and the duty cycle. As expected, a smaller gap generates a wider bandwidth. For the duty cycle, the higher duty cycle (75%) consistently shows a larger bandwidth compared to the 60% duty cycle by a few nanometers. From those results, the coupling coefficients are extracted for a comparison with the predicted values from the coupled-mode simulation and the band structure analysis. The comparison

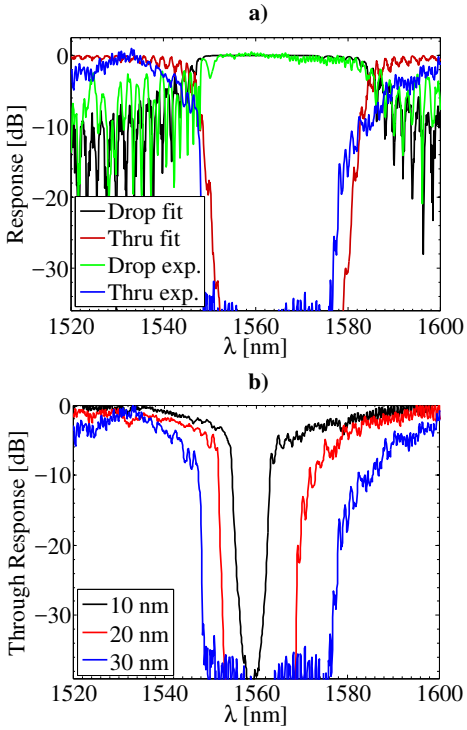

Fig. 3. (a) Experimental and simulated spectral response of the broadband filter. The 3dB bandwidth is 4.07 THz. The design has a gap of 100 nm, a duty cycle of 75%, a period of 355 nm and corrugation depths of 30 nm. (b) Effect of the corrugation depth on the bandwidth response with value of 10, 20 and 30 nm. The designs have gaps of 100 nm, duty cycles of 75% and periods of 355 nm. The 3 dB bandwidth are of 8, 20 and 33.4 nm or 1.00, 2.50 and 4.07 THz.

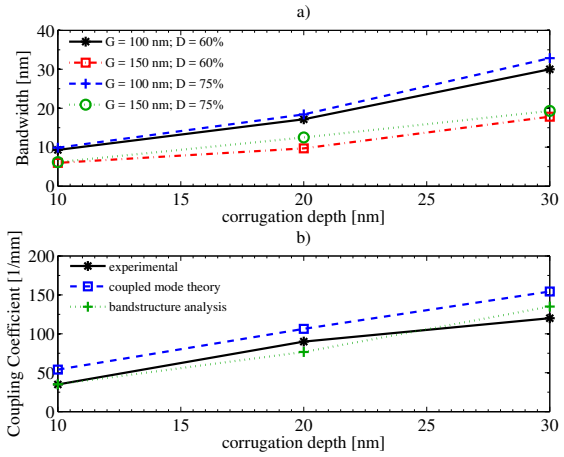

Fig. 4. (a) Bandwidth results as function of the corrugation depth for various gap (100 and 150 nm) and duty cycle (60 and 75%). (b) Coupling coefficient as function of the corrugation depth from the experimental data, the coupled mode theory simulation and the band structure analysis simulation.

is plotted in Fig.4 b). The coupled-mode simulation overestimated the coupling coefficient. The band structure analysis was more accurate with the largest error of less than 15.1 mm^{-1} compared to the experimental result while it was 34.4 mm^{-1} for the

coupled-mode simulation.

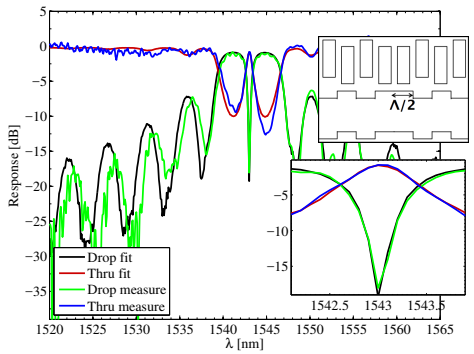

Fig. 5. Experimental and simulated spectral responses of the phased-shifted resonator device. The 3 dB bandwidth of the transmission peak is 0.86 nm. The design has a gap of 150 nm, a duty cycle of 60%, a Bragg period of 365 nm and corrugation depths of 10 nm. The insets show a schematic of the phase shift and the response at the resonance wavelength.

The introduction of a phase-shift in the center of the grating is tested as shown in Fig.5. The π phase-shift is realized by repeating half a grating period of the smaller-gap section in the Bragg grating. This allows the contra-DC to act as an optical resonator structure with a transmission peak at the center of stop band in the through port [7]. Similar to the case of broadband filter, the simulation fit of the spectrum has incorporated high-frequency noise generation and linear chirp. The spectrum is normalized to eliminate the insertion-loss uncertainty due to the grating couplers. A propagation loss of 17.5 dB/cm has been assumed in simulation to fit the measured depth of the resonant dip in the drop-port output and the bandwidth of the transmission peak. We suspect that this high loss is due to the strong corrugation. It may be reduced by optimizing the desgin paramters, such as the SWG duty cycle and corrugation depth, through further investigation. A resonator quality factor of 1,800 is extracted from the transmission peak that has a bandwidth of 0.856 nm (100 GHz) at 1543 nm. The resonant notch in the drop-port response has an extinction ratio of over 17 dB.

In this Letter, we have demonstrated a novel device using SWG waveguides in a grating-assisted contra-DC. Its bandwidth and filter shape can be largely tailored by the design of SWG (e.g., by varying the duty cycle). In particular, a 3 dB bandwidth of up to 4.07 THz has been achieved. This is to our knowledge the highest bandwidth achieved for an add-drop filter on a silicon chip. In addition, we demonstrated a resonator structure by introducing a phase-shift in the center of the grating, showing the possibility to achieve a narrow-band design in SWG contra-DC. This also provides an efficient method to extract the propagation loss for Bragg gratings and contra-DCs. Manipulating the coupling coefficient and the mode profile at nanometer scale, the use of subwavelength structures in general, and of SWG waveguides in particular, provides an additional degree of freedom in designing Bragg filters and devices. This makes the device attractive to a vast number of applications that require flexible filter designs.

FUNDING.

Natural Sciences and Engineering Research Council of Canada (NSERC).

ACKNOWLEDGMENT.

The authors thank Yun Wang and Lukas Chrostowski at the University of British Columbia for the fiber grating coupler design. The silicon chip was fabricated at Applied Nanotools Inc.

REFERENCES

1. X. Wang, W. Shi, H. Yun, S. Grist, N. A. Jaeger, and L. Chrostowski, Optics express **20**, 15547 (2012).
2. W. Bogaerts, P. De Heyn, T. Van Vaerenbergh, K. De Vos, S. Kumar Selvaraja, T. Claes, P. Dumon, P. Bienstman, D. Van Thourhout, and R. Baets, Laser & Photonics Reviews **6**, 47 (2012).
3. F. Horst, W. M. Green, S. Assefa, S. M. Shank, Y. A. Vlasov, and B. J. Offrein, Optics express **21**, 11652 (2013).
4. W. Shi, H. Yun, C. Lin, X. Wang, J. Flueckiger, N. Jaeger, and L. Chrostowski, "Silicon cwdm demultiplexers using contra-directional couplers," in "CLEO: Science and Innovations," (Optical Society of America, 2013), pp. CTu3F–5.
5. J. St-Yves, H. Bahrami, P. Jean, S. LaRochelle, and W. Shi, Optics letters **40**, 5471 (2015).
6. A. D. Simard and S. LaRochelle, Optics express **23**, 16662 (2015).
7. W. Shi, X. Wang, C. Lin, H. Yun, Y. Liu, T. Baehr-Jones, M. Hochberg, N. A. Jaeger, and L. Chrostowski, Optics express **21**, 3633 (2013).
8. P. J. Bock, P. Cheben, J. H. Schmid, J. Lapointe, A. Delâge, S. Janz, G. C. Aers, D.-X. Xu, A. Densmore, and T. J. Hall, Optics express **18**, 20251 (2010).
9. R. Halir, A. Maese-Novo, A. Ortega-Moñux, I. Molina-Fernández, J. Wangüemert-Pérez, P. Cheben, D.-X. Xu, J. Schmid, and S. Janz, Optics express **20**, 13470 (2012).
10. P. Cheben, J. H. Schmid, S. Wang, D.-X. Xu, M. Vachon, S. Janz, J. Lapointe, Y. Painchaud, and M.-J. Picard, Optics express **23**, 22553 (2015).
11. J. Wang, I. Glesk, and L. R. Chen, Optics express **22**, 15335 (2014).
12. B. Naghdi and L. R. Chen, Optics express **24**, 23429 (2016).
13. B. Liu, Y. Zhang, Y. He, X. Jiang, J. Peng, C. Qiu, and Y. Su, Optics Express **25**, 11359 (2017).
14. E. Peral and J. Capmany, Journal of lightwave technology **15**, 1295 (1997).
15. S. Rytov, Soviet Physics Jetp-Ussr **2**, 466 (1956).
16. https://kb.lumerical.com/en/diffractive_optics_pc_bandstructure.html. Retrieved on Dec. 4, 2017.
17. W. Shi, H. Yun, C. Lin, M. Greenberg, X. Wang, Y. Wang, S. T. Fard, J. Flueckiger, N. A. Jaeger, and L. Chrostowski, Optics express **21**, 6733 (2013).
18. J. D. Sarmiento-Merenguel, A. Ortega-Moñux, J.-M. Fédéli, J. G. Wangüemert-Pérez, C. Alonso-Ramos, E. Durán-Valdeiglesias, P. Cheben, Í. Molina-Fernández, and R. Halir, Optics letters **41**, 3443 (2016).
19. V. Donzella, A. Sherwali, J. Flueckiger, S. T. Fard, S. M. Grist, and L. Chrostowski, Optics express **22**, 21037 (2014).
20. Y. Wang, X. Wang, J. Flueckiger, H. Yun, W. Shi, R. Bojko, N. A. Jaeger, and L. Chrostowski, Optics express **22**, 20652 (2014).
21. X. Wang, W. Shi, M. Hochberg, K. Adam, E. Schelew, J. F. Young, N. A. Jaeger, and L. Chrostowski, "Lithography simulation for the fabrication of silicon photonic devices with deep-ultraviolet lithography," in "Group IV Photonics (GFP), 2012 IEEE 9th International Conference on," (IEEE, 2012), pp. 288–290.
22. S. K. Selvaraja, W. Bogaerts, P. Dumon, D. Van Thourhout, and R. Baets, IEEE Journal of Selected Topics in Quantum Electronics **16**, 316 (2010).
23. A. D. Simard, G. Beaudin, V. Aimez, Y. Painchaud, and S. LaRochelle, Optics express **21**, 23145 (2013).
24. N. Ayotte, A. D. Simard, and S. LaRochelle, IEEE Photonics Technol. Lett. **27**, 755 (2015).
25. P. Dumon, W. Bogaerts, V. Wiaux, J. Wouters, S. Beckx, J. Van Campenhout, D. Taillaert, B. Luyssaert, P. Bienstman, D. Van Thourhout, and R. Beats, IEEE Photonics Technology Letters **16**, 1328 (2004).